

Confinement Induced Resonances in Spherical Shell Traps

C. Moritz Carmesin^{1,*} and Maxim A. Efremov^{1,2}

¹*Institut für Quantenphysik and Center for Integrated Quantum Science and Technology (IQST), Universität Ulm, 89081 Ulm, Germany*

²*German Aerospace Center (DLR), Institute of Quantum Technologies, 89081 Ulm, Germany*

We have computed exactly the energy spectrum and corresponding wave functions of two bosonic particles, which are confined in a spherically symmetric shell-shaped trap and interact with each other via a three-dimensional zero-range potential. Confinement induced resonances (CIRs), originating entirely from the strong coupling of the relative and center-of-mass motions of the two particles, are identified as avoided crossings at certain values of the shell radius. By working close to the found CIRs, these results offer a new way to enhance the atom-atom interaction in the atomic gas by tuning only the geometrical parameters of the shell.

Introduction.— Many quantum phenomena depend crucially on the geometry and topology of the problem. For example, the simple quantum-mechanical problem of two identical, interacting particles confined in harmonic traps forming an effectively one-dimensional (1D) waveguide [1, 2], or a 2D plane [3], or a ball [4] displays remarkable changes in the binding spectrum as well as scattering properties in comparison with non-confined particles. These results opened a new avenue to control the interparticle interaction via CIRs [5, 6], by employing the harmonic confinement realized with optical fields [7]. Moreover, CIRs are universal, since they are determined solely by the geometry of the trap.

Recently ultracold atomic bubbles have attracted a lot of attention as the best candidate to test fundamental ideas in few- and many-body quantum theory and statistical mechanics in a new geometry, namely on a curved manifold [8]. In fact, there exist two successfully working schemes [9–11] for producing atomic shells in labs [12]: The first is using radio-frequency dressing [13] in a microgravity environment [14–19], while the second involves an optically confined mixture of two Bose–Einstein condensates either employing a magic laser wavelength [11, 20], or combining microgravity [21] with a Feshbach resonance [22, 23] to tune the interspecies interaction. Inspired by the availability of this novel topology, many groups have reconsidered well-known phenomena, such as Bose-Einstein condensation [24–28], the collective excitations in condensate shells [21, 29–31], vortices [32–35], and the Berezinskii-Kosterlitz-Thouless transition [36, 37], discovered previously in a flat geometry, in the case of shell-shaped gases. However, these studies did not pay attention to the effects of curvature, or external confinement onto the atom-atom interaction. As we have already learned from the pioneering works [1–3], the confinement does have a significant impact onto two-particle systems, resulting in the appearance of CIRs. Here, we show that the shell trap allows to enhance atom-atom interaction in shell-shaped quantum gases, not with magnetic fields but with the geometrical parameters of the shell trap. This is most applicable for large thin shells, where the atom-atom interaction energy, being proportional to the atom density, decreases as $1/r_0^2$ with increasing shell radius r_0 .

In this Letter, we show that in the shell-shaped trap many CIRs appear at certain *shell radii* r_0 . By computing exactly the energy spectrum and the corresponding wave functions of

two bosonic particles, which are confined in the shell-shaped trap and interact with each other via a 3D zero-range potential characterized by the s -wave scattering length a_0 , we determine the position and width of CIRs as a function of a_0 and r_0 . The found CIRs are identified as avoided crossings between a bound (molecular) state with excitation of the center-of-mass (CoM) motion and a trap (non-molecular) state without CoM excitation, as well as between two trap states. These resonances originate entirely from the strong coupling of the relative and CoM motions of the two particles, similar to CIRs [38, 39] induced by the anharmonicity of the trap, or heteronuclear atoms in a harmonic confinement [40–42]. Hence, when changing slowly the shell radius r_0 around a bound-trap CIR, the two particles can form a molecule without requiring a third particle, since the binding energy can be transferred to the CoM degrees of freedom. The formation of molecules is a basic loss mechanism and provides a scheme to observe such bound-trap CIRs and therefore to explore the stability of the atomic bubble. In addition, the found trap-trap CIRs are of great importance to model correctly the effective atom-atom interaction, while performing a dimensional reduction of the BEC dynamics from 3D to 2D curved manifolds [43].

Two Particles in a Spherical Shell Trap.— We consider two identical bosons of mass m , which are trapped in a shell potential [30] modeled as a spherically symmetric shifted harmonic oscillator $V_0(\mathbf{r}_i) = \frac{1}{2}m\omega^2(|\mathbf{r}_i| - r_0)^2$, where $i = 1$ or 2 , with the trap frequency ω and the shift r_0 of the potential minimum. Instead of the commonly used Fermi-Huang three-dimensional pseudopotential we model the interparticle interaction by a Bethe-Peierls boundary condition [44] for the two-particle wave function Ψ , that is

$$\lim_{r_1 \rightarrow r_2} \left\{ \frac{\partial [|\mathbf{r}_1 - \mathbf{r}_2| \Psi(\mathbf{r}_1, \mathbf{r}_2)]}{\partial |\mathbf{r}_1 - \mathbf{r}_2|} + \frac{|\mathbf{r}_1 - \mathbf{r}_2|}{a_0} \Psi(\mathbf{r}_1, \mathbf{r}_2) \right\} = 0 \quad (1a)$$

for partial waves with zero relative angular momentum, $\ell = 0$, and

$$\lim_{r_1 \rightarrow r_2} |\mathbf{r}_1 - \mathbf{r}_2| \Psi(\mathbf{r}_1, \mathbf{r}_2) = 0 \quad (1b)$$

for partial waves with the relative angular momentum $\ell > 0$.

In the case of an ordinary spherically symmetric harmonic confinement, that is $r_0 = 0$, both the Hamiltonian

$$\hat{H} = -\frac{\hbar^2}{2m} (\Delta_{\mathbf{r}_1} + \Delta_{\mathbf{r}_2}) + V_0(\mathbf{r}_1) + V_0(\mathbf{r}_2) \quad (2)$$

of our system and the boundary conditions, Eqs. (1a) and (1b), are separable in terms of the relative $\mathbf{r} = \mathbf{r}_1 - \mathbf{r}_2$ and CoM $\mathbf{R} = \frac{1}{2}(\mathbf{r}_1 + \mathbf{r}_2)$ coordinates and the two-particle energy spectrum can be derived analytically [4]. Here Δ_r denotes the three-dimensional Laplace operator. In this Letter, we however consider the case of $r_0 > 0$ and the Hamiltonian is not anymore separable in terms of the \mathbf{r} and \mathbf{R} coordinates.

To solve the resulting six-dimensional stationary Schrödinger equation $\hat{H}\Psi = E\Psi$ for the two-particle wave function Ψ with the corresponding two-particle energy E exactly, we perform numerical computations in terms of the relative and CoM coordinates by applying a two-step approach [45]. First, we compute a set of basis functions: the CoM wave functions are the eigenfunctions of the shifted radial harmonic oscillator with Dirichlet boundary condition, whereas the relative wave functions are those of a radially symmetric harmonic oscillator, but obeying the boundary conditions given by Eqs. (1a) and (1b). Second, we represent the Hamiltonian \hat{H} in terms of these radial basis functions, combined with spherical harmonics for the angular degrees of freedom. The resulting matrix is finally diagonalized. The utilized basis functions are very useful, since only a few of them are actually needed to obtain the exact solution.

Due to a strong coupling between CoM and relative motions, it is essential to find and work in the coordinates where the couplings between different degrees of freedom are negligible, leading to a reduction of the dimensionality of the problem. For our physical system, this is achieved with the hyperspherical coordinates [46]: the hyperradius $\xi = \sqrt{\frac{1}{2}r^2 + 2R^2}$, the hyperangle $\chi = \arctan(r/2R)$, the spherical angles θ and ϕ of \mathbf{r} , as well as Θ and Φ of \mathbf{R} .

In these coordinates the Hamiltonian, Eq. (2), reads

$$\hat{H} = -\frac{\hbar^2}{2m} \left(\frac{\partial^2}{\partial \xi^2} + \frac{5}{\xi} \frac{\partial}{\partial \xi} - \frac{\hat{\Lambda}^2}{\xi^2} \right) + \frac{m\omega^2}{2} (\xi - \xi_0)^2 + \mathcal{V}_c, \quad (3)$$

where $\xi_0 = \sqrt{2}r_0$ and the operator $\hat{\Lambda}^2 = -\hat{\Lambda}_0^2 + \mathcal{W}_\xi(\chi)$ consists of the Laplacian

$$\hat{\Lambda}_0^2 = \frac{\partial^2}{\partial \chi^2} + 4 \cot(2\chi) \frac{\partial}{\partial \chi} - \frac{\hat{\ell}^2}{\sin^2(\chi)} - \frac{\hat{L}^2}{\cos^2(\chi)} \quad (4)$$

on the six-dimensional hypersphere with the relative $\hat{\ell}^2$ and CoM \hat{L}^2 orbital angular momentum operators, and the potential

$$\mathcal{W}_\xi(\chi) = \frac{2\xi^3 \xi_0}{a_{\text{ho}}^4} \left[1 - \frac{2 + \sin^2(2|\frac{\pi}{4} - \chi|)}{3 \cos(\frac{\pi}{4} - |\frac{\pi}{4} - \chi|)} \right] \quad (5)$$

with the characteristic length $a_{\text{ho}} \equiv \sqrt{\hbar/(m\omega)}$ of the shell-shaped trapping potential $V_0(\mathbf{r})$, defining also the shell width.

The last term in Eq. (3)

$$\mathcal{V}_c = -m\omega^2 \xi \xi_0 \sum_{l=1}^{\infty} \frac{\sin^{2l}(\frac{\pi}{4} - |\chi - \frac{\pi}{4}|)}{\cos^{2l+1}(\frac{\pi}{4} - |\chi - \frac{\pi}{4}|)} \left[\frac{\sin^2(\frac{\pi}{4} - |\chi - \frac{\pi}{4}|)}{4l+3} - \frac{\cos^2(\frac{\pi}{4} - |\chi - \frac{\pi}{4}|)}{4l-1} \right] \frac{4\pi}{4l+1} \sum_{\mu=-2l}^{2l} Y_{2l,\mu}(\theta, \phi) Y_{2l,\mu}^*(\Theta, \Phi), \quad (6)$$

with $Y_{l,m}$ being the spherical harmonics on the three-dimensional sphere, couples all degrees of freedom.

In the hyperspherical coordinates, the boundary conditions, Eqs. (1a) and (1b), take the simpler form

$$\frac{1}{\sin(2\chi)\Psi} \frac{d}{d\chi} [\sin(2\chi)\Psi] \Big|_{\chi \rightarrow 0} = -\frac{\sqrt{2}\xi}{a_0} \quad \text{for } \ell = 0 \quad (7a)$$

$$\sin(2\chi)\Psi \Big|_{\chi \rightarrow 0} = 0 \quad \text{for } \ell > 0. \quad (7b)$$

When we neglect the coupling potential \mathcal{V}_c , the angular variables of the relative (θ and ϕ) and CoM (Θ and Φ) motions are separated from each other as well as from the hyperradius ξ and hyperangle χ both in the Hamiltonian, Eq. (3), and the boundary conditions, Eqs. (7a) and (7b). In this way, Eq. (3) would have the form of a spherically symmetric six-dimensional radially shifted harmonic oscillator, if the operator $\hat{\Lambda}^2$ and the boundary conditions, Eqs. (7a) and (7b), were ξ -independent. However, this is not the case and we have to use a proper scheme to solve the reduced two-dimensional Schrödinger equation numerically. This is done approximately [45] within the adiabatic approximation. Namely, we first compute the eigenvalues $\lambda(n_\chi, L, \ell; \xi)$ and eigenfunctions $V_{n_\chi L \ell, \xi}(\chi)$ of the operator $\hat{\Lambda}^2$ taking into account Eqs. (7a) and (7b), with ξ considered as a parameter. We then replace $\hat{\Lambda}^2$ in Eq. (3) by λ , neglect the coupling \mathcal{V}_c and solve the obtained eigenvalue equation for the hyperradial wave functions $U_{n_\xi n_\chi L \ell}(\xi)$ and the corresponding two-particle energies $E_{n_\xi n_\chi L \ell}$.

Energy Spectrum.— In this Letter, we restrict our analysis to the two-particle states with zero total angular momentum, that is with $L = 0$ and $\ell = 0$. Therefore, the uncoupled (approximate) states can be labeled as $|n_\xi n_\chi\rangle$, where n_ξ and n_χ denote the number of nodes of the wave function along the hyperradial and hyperangular directions, respectively. In contrast, we have to label the exact (coupled) states $|n\rangle$ by a single index n . For the scattering length $a_0 = 0.5a_{\text{ho}}$, we present in the upper panel of Fig. 1 the dependence of the corresponding two-particle energies E on the shell radius r_0 , obtained with exact (solid lines) and approximate (dotted lines) methods [45].

Starting from $r_0 = 0$ the energies $E_{n_\xi n_\chi}(r_0)$ and $E_n(r_0)$ decrease rapidly with increasing shift r_0 and then saturate. This can be related to the transition of a three-dimensional harmonic oscillator to an effectively one-dimensional one for sufficiently large shell radii. Indeed, at $r_0 = 0$ the two-body spectrum is exactly given by the spectrum of a three-dimensional harmonic oscillator

$$E_{n_\xi n_\chi} = \left[\mathcal{E}_{n_\chi}(a_0) + 2n_\xi + \frac{3}{2} \right] \hbar\omega \quad (8)$$

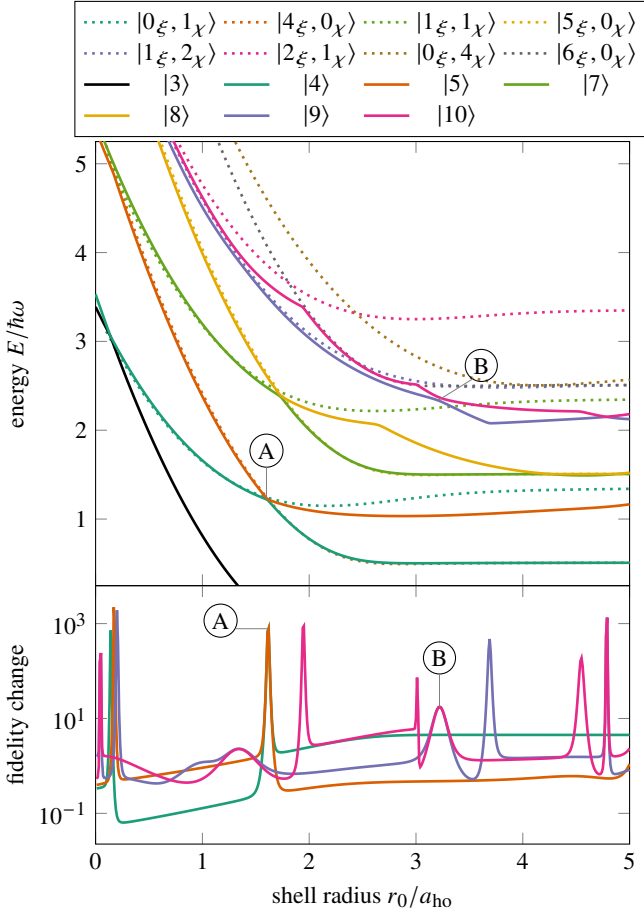


Figure 1. (color online) The exact (E_n) and approximated ($E_{n_\xi n_\chi}$) two-particle energies (upper panel) and fidelity change $\delta\mathcal{F}_n$ (lower panel) as functions of the shell radius r_0 for selected low energy states with zero total angular momentum and the scattering length $a_0 = 0.5a_{ho}$. We show the energies obtained from the exact six-dimensional computation (solid lines) and approximate approach based on the hyperspherical coordinates (dotted lines). The two marked avoided crossings (A): $|0_\xi 1_\chi\rangle$ (dark green) with $|4_\xi 0_\chi\rangle$ (orange), and (B): $|1_\xi 2_\chi\rangle$ (purple) with $|0_\xi 4_\chi\rangle$ (pink), are analyzed in detail. The full low-energy spectrum is presented in [45, Fig. S.1], where we also show that AC (A) is the energetically lowest one for the given a_0 .

shifted by the dimensionless energies \mathcal{E}_{n_χ} of the hyperangular motion, which is reduced to the relative motion for $r_0 = 0$. The hyperangular energies are determined by the roots of the transcendental equation [4]

$$\sqrt{2} \frac{\Gamma\left(\frac{3}{4} - \frac{1}{2}\mathcal{E}_{n_\chi}\right)}{\Gamma\left(\frac{1}{4} - \frac{1}{2}\mathcal{E}_{n_\chi}\right)} = -\frac{a_{ho}}{a_0}. \quad (9)$$

For $0 < a_0/a_{ho} < 1$ and $n_\chi = 0$, we have obtained [45] $\mathcal{E}_0 = -(a_{ho}/a_0)^2 + (1/8)(a_0/a_{ho})^2 + \mathcal{O}\left[(a_0/a_{ho})^6\right]$. However, for $r_0 \gg a_{ho}$, the bound-state energies feature the spectrum of

the one-dimensional harmonic oscillator [45]

$$E_{n_\xi 0} \approx \left[\mathcal{E}_0(a_0) + n_\xi + \frac{1}{2} \right] \hbar\omega, \quad (10)$$

that is also shifted by the hyperangular bound-state energy $\mathcal{E}_0 = -(a_{ho}/a_0)^2 + (1/24)(a_0/a_{ho})^2 + \mathcal{O}\left[(a_0/a_{ho})^6\right]$, valid for $0 < a_0/a_{ho} < 1$.

Moreover, for intermediate shell radii r_0 the energy spectrum displays many crossings and avoided crossings (AC). In general, their positions and widths are determined by both r_0 and a_0 . To identify and determine the former properties of the ACs, corresponding to CIRs [5, 6, 39], we analyze the fidelity change [47, 48]

$$\delta\mathcal{F}_n(r_0) = \frac{1 - \langle n(r_0)|n(r_0 + \delta r_0)\rangle}{(\delta r_0/a_{ho})^2} \quad (11)$$

of the exact eigenstates $|n\rangle$ as a function of r_0 for a given a_0 . As clearly shown in the lower panel of Fig. 1, $\delta\mathcal{F}_n(r_0)$ exhibits peaks. When the peaks of the fidelity change $\delta\mathcal{F}_{n_1}$ of the state $|n_1\rangle$ and $\delta\mathcal{F}_{n_2}$ of the state $|n_2\rangle$ coincide, the constituent states of the AC are identified. Further, we can determine the position and width of the AC from these peaks.

Confinement-Induced Resonances.— We now consider in detail two kinds of avoided crossings, labeled by (A) and (B) in Fig. 1, respectively. In Fig. 2 a), we display the details of AC (A), which couples the states $|4_\xi 0_\chi\rangle$, shown in the top left inset by the density plot of $|\langle r, R|5\rangle|^2$, and $|0_\xi 1_\chi\rangle$, shown in the bottom left inset by the density plot of $|\langle r, R|4\rangle|^2$. Since we consider here the two-particle states with $L = 0$ and $\ell = 0$, the density plots are only functions of the distances R and r . The state $|4_\xi 0_\chi\rangle$ does not feature the hyperradial symmetry but is tightly localized at small relative distances r . Actually, it resembles a bound state of non-trapped particles with the characteristic exponential decay $\exp(-r/a_0)$. Such a state corresponds to a molecule on the shell or a *bound state* of two particles. These states only appear for positive a_0 and exhibit the molecular form only for small positive a_0/a_{ho} , since otherwise the trap potential dominates. The second state $|0_\xi 1_\chi\rangle$ of AC (A), possesses the hyperradial symmetry, which is dictated by the trap structure. We denote such states as *trap states* of two particles. Avoided crossings, such as (A), describe an interplay between the molecular and trap states, are named here as *bound-trap* CIRs.

The second kind of CIRs is exemplified by AC (B), which is displayed in Fig. 2 b). Here, the state $|0_\xi 4_\chi\rangle$, depicted in the top left inset by the density plot of $|\langle r, R|10\rangle|^2$, is coupled to the state $|1_\xi 2_\chi\rangle$, depicted in the bottom left inset by the density plot of $|\langle r, R|9\rangle|^2$. Since neither of the involved states is a molecular one, we call such ACs *trap-trap* CIRs. We emphasize, that both kind of resonances originate entirely from the strong coupling between the CoM and relative motions.

In Fig. 3 the positions of the AC (A) and other two bound-trap CIRs (dots), as well as the AC (B) (squares) are presented in the

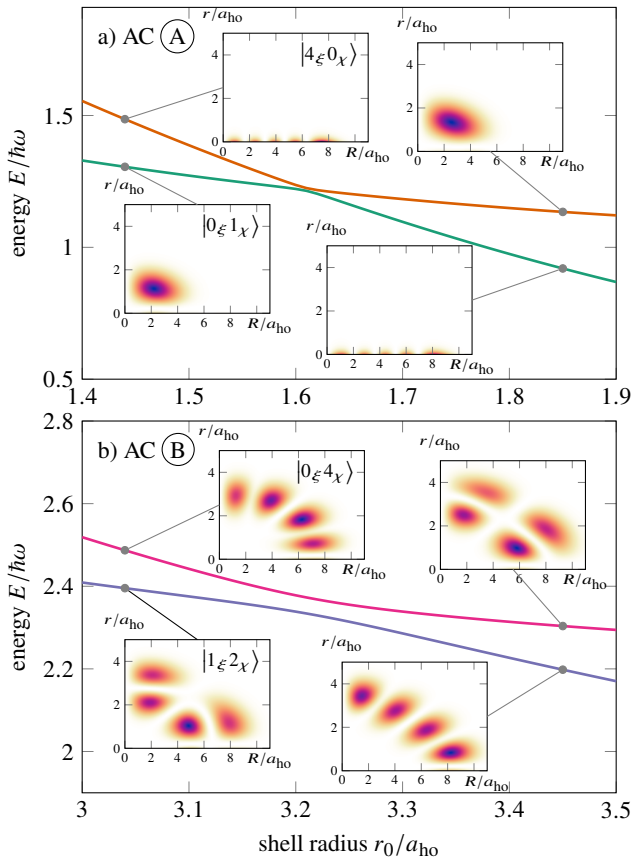


Figure 2. (color online) Magnifications of the energy levels at the labeled avoided crossings (A) and (B), Fig. 1, together with the density $|\langle r, R|n\rangle|^2$ of the involved states before and after the avoided crossing. In panel a), the avoided crossing (A) couples the molecule state $|0_\xi 1_\chi\rangle$ with the excited trap one $|4_\xi 0_\chi\rangle$ and represents a bound-trap CIR. In panel b) the trap state $|0_\xi 4_\chi\rangle$ with excitation in χ direction has the avoided crossing (B) with the trap state $|1_\xi 2_\chi\rangle$ having excitations in both ξ and χ directions.

parameter space of the scattering length a_0 and the shell radius r_0 . The positions of the bound-trap CIRs strongly depend on a_0 , since the energy of the molecular state and hence the level spacing of the involved states are crucially determined by the value of a_0 . Consequently, a given trap state avoids crossing with the corresponding molecular state only in a small interval of a_0 and with increasing a_0 the position of this AC becomes shifted towards larger shell radii until it disappears. Note that close before the vanishing of AC the curve in the r_0 - a_0 plane becomes nearly horizontal (here only resolved for the purple AC). This behavior is due to the fact that the involved energy levels become nearly parallel for large r_0 , as depicted in Fig. 1. In contrast, the positions of trap-trap ACs like AC (B) are nearly independent of a_0 , as the shape and the energy level spacing of the involved trap states are essentially unaffected by a change of the scattering length.

Summary and outlook.— We have computed the energy spectrum and corresponding wave functions of two bosonic

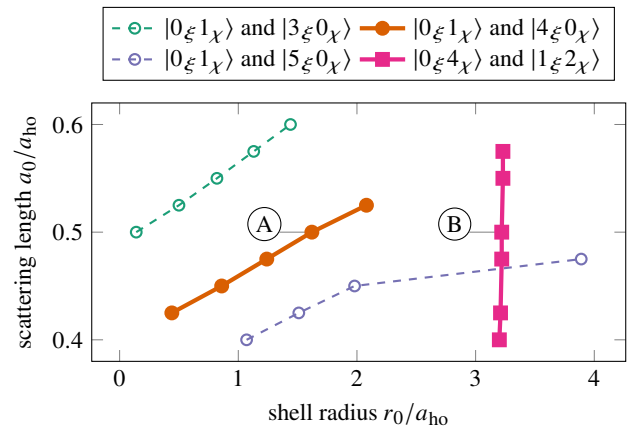


Figure 3. Positions of selected avoided crossings of low-energy states with zero total angular momentum in the a_0 - r_0 parameter space. The circles mark bound-trap ACs, similar to (A) (orange). Due to strong dependence of energy of the molecular state on a_0 , a given bound-trap AC only appears for a narrow interval of a_0 before another AC with the next lower (turquoise), or higher (purple) trap state arises, taking finally its place. In contrast, trap-trap ACs (squares), similar to (B), dependent weakly on a_0 and strongly on r_0 , resulting from the weak dependence on a_0 and strong dependence r_0 of the energy levels spacing of the involved states.

particles, which are confined in a spherically symmetric shell-shaped trap and interact with each other through a 3D zero-range potential. Here we have identified CIRs as avoided crossings between the bound (molecular) state with CoM excitation and trap (non-molecular) state without CoM excitation, as well as between two trap states. We determined the positions and widths of these resonances that arise due to the strong coupling of the relative and CoM motions of the two particles. In this way, an adiabatic change of the shell radius around a bound-trap CIR can be employed to drive the formation of a molecule in the shell-shaped atomic gas. The subsequent collisions of the formed molecules with each other, or with other atoms lead to creation of the tighter molecules and fast atoms, that is losses in the shell-shaped atomic gas. For a shell potential realized with the rf-dressing technique [13], the shell radius r_0 can be changed adiabatically via varying slowly the rf-detuning Δ , because $r_0 \propto \sqrt{\Delta}$. For a shell potential created with dual-species atomic mixture [11, 21], the time-dependent shell radius can be realized for instance during free expansion. Reversely, these two cases present two ways to probe the found bound-trap CIRs via observing losses. Additionally, it would be great of interest to explore CIRs appearing also in ring-shaped quantum gases [49], as they have useful applications in building compact sensors for inertial and non-inertial forces.

We thank A. Wolf for fruitful discussions and helpful suggestions.

* moritz.carmesin@uni-ulm.de

- [1] M. Olshanii, Atomic scattering in the presence of an external confinement and a gas of impenetrable bosons, *Phys. Rev. Lett.* **81**, 938 (1998).
- [2] T. Bergeman, M. G. Moore, and M. Olshanii, Atom-atom scattering under cylindrical harmonic confinement: Numerical and analytic studies of the confinement induced resonance, *Phys. Rev. Lett.* **91**, 163201 (2003).
- [3] D. S. Petrov, M. Holzmann, and G. V. Shlyapnikov, Bose-einstein condensation in quasi-2d trapped gases, *Phys. Rev. Lett.* **84**, 2551 (2000).
- [4] T. Busch, B.-G. Englert, K. Rzazewski, and M. Wilkens, Two cold atoms in a harmonic trap, *Foundations of Physics* **28**, 549 (1998).
- [5] V. Dunjko, M. G. Moore, T. Bergeman, and M. Olshanii, *Advances in Atomic, Molecular, and Optical Physics*, edited by E. Arimondo, P. Berman, and C. Lin, *Advances In Atomic, Molecular, and Optical Physics*, Vol. 60 (Academic Press, 2011) pp. 461–510.
- [6] C. H. Greene, P. Giannakeas, and J. Pérez-Ríos, Universal few-body physics and cluster formation, *Rev. Mod. Phys.* **89**, 035006 (2017).
- [7] I. Bloch, J. Dalibard, and W. Zwerger, Many-body physics with ultracold gases, *Rev. Mod. Phys.* **80**, 885 (2008).
- [8] A. Tononi and L. Salasnich, Low-dimensional quantum gases in curved geometries, *Nature Reviews Physics* **5**, 398 (2023).
- [9] R. A. Carollo, D. C. Aveline, B. Rhyno, S. Vishveshwara, C. Lannert, J. D. Murphree, E. R. Elliott, J. R. Williams, R. J. Thompson, and N. Lundblad, Observation of ultracold atomic bubbles in orbital microgravity, *Nature* **606**, 281 (2022).
- [10] Y. Guo, E. M. Gutierrez, D. Rey, T. Badr, A. Perrin, L. Longchambon, V. S. Bagnato, H. Perrin, and R. Dubessy, Expansion of a quantum gas in a shell trap, *New Journal of Physics* **24**, 093040 (2022).
- [11] F. Jia, Z. Huang, L. Qiu, R. Zhou, Y. Yan, and D. Wang, Expansion Dynamics of a Shell-Shaped Bose-Einstein Condensate, *Physical Review Letters* **129**, 243402 (2022).
- [12] N. Lundblad, D. C. Aveline, A. Balaž, E. Bentine, N. P. Bigelow, P. Boegel, M. A. Efremov, N. Gaaloul, M. Meister, M. Olshanii, C. A. R. S. de Melo, A. Tononi, S. Vishveshwara, A. C. White, A. Wolf, and B. M. Garraway, Perspective on quantum bubbles in microgravity, *Quantum Science and Technology* **8**, 024003 (2023).
- [13] H. Perrin and B. M. Garraway, Chapter four - trapping atoms with radio frequency adiabatic potentials (Academic Press, 2017) pp. 181–262.
- [14] D. C. Aveline, J. R. Williams, E. R. Elliott, C. Dutenhoffer, J. R. Kellogg, J. M. Kohel, N. E. Lay, K. Oudrhiri, R. F. Shotwell, N. Yu, and R. J. Thompson, Observation of bose-einstein condensates in an earth-orbiting research lab, *Nature* **582**, 193 (2020).
- [15] N. J. Penley, C. P. Schafer, and J.-D. F. Bartoe, The international space station as a microgravity research platform, *Acta Astronautica* **50**, 691 (2002).
- [16] M. Raudonis, A. Roura, M. Meister, C. Lotz, L. Overmeyer, S. Herrmann, A. Gierse, C. Lämmerzahl, N. P. Bigelow, M. Lachmann, B. Piest, N. Gaaloul, E. M. Rasel, C. Schubert, W. Herr, C. Deppner, H. Ahlers, W. Ertmer, J. R. Williams, N. Lundblad, and L. Wörner, Microgravity facilities for cold atom experiments, *Quantum Science and Technology* **8**, 044001 (2023).
- [17] T. van Zoest, N. Gaaloul, Y. Singh, H. Ahlers, W. Herr, S. T. Seidel, W. Ertmer, E. Rasel, M. Eckart, E. Kajari, S. Arnold, G. Nandi, W. P. Schleich, R. Walser, A. Vogel, K. Sengstock, K. Bongs, W. Lewoczko-Adamczyk, M. Schiemangk, T. Schuldt, A. Peters, T. Kōnemann, H. Müntinga, C. Lämmerzahl, H. Dittus, T. Steinmetz, T. W. Hänsch, and J. Reichel, Bose-einstein condensation in microgravity, *Science* **328**, 1540 (2010), <https://www.science.org/doi/pdf/10.1126/science.1189164>.
- [18] C. Lotz, Y. Wessargues, J. Hermsdorf, W. Ertmer, and L. Overmeyer, Novel active driven drop tower facility for microgravity experiments investigating production technologies on the example of substrate-free additive manufacturing, *Advances in Space Research* **61**, 1967 (2018).
- [19] Frye, Kai, Abend, Sven, Bartosch, Wolfgang, Bawamia, Ahmad, Becker, Dennis, Blume, Holger, Braxmaier, Claus, Chiow, Sheng-Wey, Efremov, Maxim A., Ertmer, Wolfgang, Fierlinger, Peter, Franz, Tobias, Gaaloul, Naceur, Grosse, Jens, Grzeschik, Christoph, Hellmig, Ortwin, Henderson, Victoria A., Herr, Waldemar, Israelsson, Ulf, Kohel, James, Krutzik, Markus, Kürbis, Christian, Lämmerzahl, Claus, List, Meike, Lüdtkke, Daniel, Lundblad, Nathan, Marburger, J. Pierre, Meister, Matthias, Mihm, Moritz, Müller, Holger, Müntinga, Hauke, Nepal, Ayush M., Oberschulte, Tim, Papakonstantinou, Alexandros, Perovs, Jaka, Peters, Achim, Prat, Arnau, Rasel, Ernst M., Roura, Albert, Sbroscia, Matteo, Schleich, Wolfgang P., Schubert, Christian, Seidel, Stephan T., Sommer, Jan, Spindeldreier, Christian, Stamper-Kurn, Dan, Stuhl, Benjamin K., Warner, Marvin, Wendrich, Thijs, Wenzlawski, André, Wicht, Andreas, Windpassinger, Patrick, Yu, Nan, and Wörner, Lisa, The bose-einstein condensate and cold atom laboratory, *EPJ Quantum Technol.* **8**, 1 (2021).
- [20] M. Meister and A. Roura, Efficient matter-wave lensing of ultracold atomic mixtures, *Quantum Science and Technology* **8**, 024001 (2023).
- [21] A. Wolf, P. Boegel, M. Meister, A. Balaž, N. Gaaloul, and M. A. Efremov, Shell-shaped bose-einstein condensates based on dual-species mixtures, *Phys. Rev. A* **106**, 013309 (2022).
- [22] C. Chin, R. Grimm, P. Julienne, and E. Tiesinga, Feshbach resonances in ultracold gases, *Rev. Mod. Phys.* **82**, 1225 (2010).
- [23] E. Timmermans, P. Tommasini, M. Hussein, and A. Kerman, Feshbach resonances in atomic bose-einstein condensates, *Physics Reports* **315**, 199 (1999).
- [24] F. Dalfovo, S. Giorgini, L. P. Pitaevskii, and S. Stringari, Theory of bose-einstein condensation in trapped gases, *Rev. Mod. Phys.* **71**, 463 (1999).
- [25] A. Tononi and L. Salasnich, Bose-einstein condensation on the surface of a sphere, *Phys. Rev. Lett.* **123**, 160403 (2019).
- [26] N. S. Möller, F. E. A. dos Santos, V. S. Bagnato, and A. Pelster, Bose-einstein condensation on curved manifolds, *New Journal of Physics* **22**, 063059 (2020).
- [27] A. Tononi, F. Cinti, and L. Salasnich, Quantum bubbles in microgravity, *Phys. Rev. Lett.* **125**, 010402 (2020).
- [28] B. Rhyno, N. Lundblad, D. C. Aveline, C. Lannert, and S. Vishveshwara, Thermodynamics in expanding shell-shaped bose-einstein condensates, *Phys. Rev. A* **104**, 063310 (2021).
- [29] C. Lannert, T.-C. Wei, and S. Vishveshwara, Dynamics of condensate shells: Collective modes and expansion, *Phys. Rev. A* **75**, 013611 (2007).
- [30] K. Sun, K. Padavić, F. Yang, S. Vishveshwara, and C. Lannert, Static and dynamic properties of shell-shaped condensates, *Phys. Rev. A* **98**, 013609 (2018).
- [31] K. Padavić, K. Sun, C. Lannert, and S. Vishveshwara, Physics of hollow bose-einstein condensates, *Europhysics Letters* **120**, 20004 (2018).
- [32] A. L. Fetter, Rotating trapped bose-einstein condensates, *Rev. Mod. Phys.* **81**, 647 (2009).
- [33] A. M. Turner, V. Vitelli, and D. R. Nelson, Vortices on curved surfaces, *Rev. Mod. Phys.* **82**, 1301 (2010).
- [34] K. Padavić, K. Sun, C. Lannert, and S. Vishveshwara, Vortex-antivortex physics in shell-shaped bose-einstein condensates,

- Phys. Rev. A **102**, 043305 (2020).
- [35] S. J. Bereta, M. A. Caracanhas, and A. L. Fetter, Superfluid vortex dynamics on a spherical film, *Phys. Rev. A* **103**, 053306 (2021).
- [36] J. M. Kosterlitz, Kosterlitz–thouless physics: a review of key issues, *Reports on Progress in Physics* **79**, 026001 (2016).
- [37] A. Tononi, A. Pelster, and L. Salasnich, Topological superfluid transition in bubble-trapped condensates, *Phys. Rev. Res.* **4**, 013122 (2022).
- [38] S. Sala, P.-I. Schneider, and A. Saenz, Inelastic confinement-induced resonances in low-dimensional quantum systems, *Phys. Rev. Lett.* **109**, 073201 (2012).
- [39] S. Sala and A. Saenz, Theory of inelastic confinement-induced resonances due to the coupling of center-of-mass and relative motion, *Phys. Rev. A* **94**, 022713 (2016).
- [40] V. Peano, M. Thorwart, C. Mora, and R. Egger, Confinement-induced resonances for a two-component ultracold atom gas in arbitrary quasi-one-dimensional traps, *New Journal of Physics* **7**, 192 (2005).
- [41] S. Grishkevich and A. Saenz, Influence of a tight isotropic harmonic trap on photoassociation in ultracold homonuclear alkali-metal gases, *Phys. Rev. A* **76**, 022704 (2007).
- [42] V. S. Melezhik and P. Schmelcher, Quantum dynamics of resonant molecule formation in waveguides, *New Journal of Physics* **11**, 073031 (2009).
- [43] N. S. Möller, F. E. A. dos Santos, V. S. Bagnato, and A. Pelster, Bose–einstein condensation on curved manifolds, *New Journal of Physics* **22**, 063059 (2020).
- [44] H. Bethe, R. Peierls, and D. R. Hartree, Quantum theory of the dipton, *Proc. R. Soc. A* **148**, 146 (1935).
- [45] See Supplemental Material attached at the end of this letter for a detailed description of the exact and approximate numerical solutions of the Schrödinger equation for the two-particle wave function, as well as the derivation of the asymptotic expansions for the two-particle energies.
- [46] T. K. Das, *Hyperspherical Harmonics Expansion Techniques: Application to Problems in Physics*, 1st ed., Theoretical and Mathematical Physics (Springer-Verlag, 2015).
- [47] P. Plötz, M. Lubasch, and S. Wimberger, Detection of avoided crossings by fidelity, *Physica A: Statistical Mechanics and its Applications* **390**, 1363 (2011).
- [48] P. Plötz, *Complex Dynamics of Ultracold Atoms*, Ph.D. thesis, Universität Heidelberg (2010).
- [49] L. Amico, D. Anderson, M. Boshier, J.-P. Brantut, L.-C. Kwek, A. Minguzzi, and W. von Klitzing, Colloquium: Atomtronic circuits: From many-body physics to quantum technologies, *Rev. Mod. Phys.* **94**, 041001 (2022).

Supplemental Material to: Confinement Induced Resonances in Spherical Shell Traps

C. Moritz Carmesin^{1,*} and Maxim A. Efremov^{1,2}

¹*Institut für Quantenphysik and Center for Integrated Quantum Science and Technology (IQST), Universität Ulm, 89081 Ulm, Germany*

²*German Aerospace Center (DLR), Institute of Quantum Technologies, 89081 Ulm, Germany*

NUMERICAL SOLUTION

In order to obtain the exact numerical solution of the stationary Schrödinger equation for the two-particle wave function, we use the spherical coordinate representation for the relative \mathbf{r} and CoM \mathbf{R} coordinates scaled in terms of the oscillator length $a_{\text{ho}} = \sqrt{\hbar/(m\omega)}$, that is $\mathbf{r} = \{a_{\text{ho}}\rho, \theta, \phi\}$ and $\mathbf{R} = \{a_{\text{ho}}\mathcal{R}, \Theta, \Phi\}$. The Hamiltonian then reads

$$\hat{H} = -\frac{1}{4}\nabla_{\mathcal{R}}^2 - \nabla_{\rho}^2 + \mathcal{R}^2 + \frac{1}{4}\rho^2 - s \left(\sqrt{\mathcal{R}^2 + \frac{1}{4}\rho^2 + \mathcal{R}\rho \cos \theta_{r\mathcal{R}}} + \sqrt{\mathcal{R}^2 + \frac{1}{4}\rho^2 - \mathcal{R}\rho \cos \theta_{r\mathcal{R}}} \right) + s^2, \quad (\text{S.1})$$

where $s = r_0/a_{\text{ho}}$ and $\theta_{r\mathcal{R}}$ is the angle between \mathbf{r} and \mathbf{R} . By representing the sum of the two square roots [1]

$$w \equiv \sqrt{\mathcal{R}^2 + \frac{1}{4}\rho^2 + \mathcal{R}\rho \cos \theta_{r\mathcal{R}}} + \sqrt{\mathcal{R}^2 + \frac{1}{4}\rho^2 - \mathcal{R}\rho \cos \theta_{r\mathcal{R}}} = \sum_{l=0}^{\infty} \left(\frac{2a^{2l}}{b^{2l+1}} \right) \left(\frac{a^2}{4l+3} - \frac{b^2}{4l-1} \right) P_{2l}(\cos \theta_{r\mathcal{R}}) \quad (\text{S.2})$$

in terms of the Legendre polynomials $P_{2l}(\cos \theta_{r\mathcal{R}})$, with $a = \min\{\frac{1}{2}\rho, \mathcal{R}\}$ and $b = \max\{\frac{1}{2}\rho, \mathcal{R}\}$, we can recast the Hamiltonian into the form

$$\hat{H} = \hat{H}_0 + s\hat{W} = \hat{H}_{\mathcal{R}} + \hat{H}_{\rho} + s\hat{W} \quad (\text{S.3})$$

with

$$\hat{H}_{\mathcal{R}} = -\frac{1}{4} \left(\frac{\partial^2}{\partial \mathcal{R}^2} + \frac{2}{\mathcal{R}} \frac{\partial}{\partial \mathcal{R}} - \frac{\hat{L}^2}{\mathcal{R}^2} \right) + (\mathcal{R} - s)^2 \quad (\text{S.4})$$

$$\hat{H}_{\rho} = - \left(\frac{\partial^2}{\partial \rho^2} + \frac{2}{\rho} \frac{\partial}{\partial \rho} - \frac{\hat{\ell}^2}{\rho^2} \right) + \frac{1}{4}\rho^2 \quad (\text{S.5})$$

$$\hat{W} = -w + 2\mathcal{R}, \quad (\text{S.6})$$

where \hat{L} and $\hat{\ell}$ are the angular momentum operators for the CoM and relative motion, respectively. In addition, the particle-particle s -wave interaction is assumed to be well described by the Bethe-Peierls boundary condition

$$\frac{1}{\rho\Psi(\rho, \mathcal{R})} \frac{d}{d\rho} [\rho\Psi(\rho, \mathcal{R})] \Big|_{\rho \rightarrow 0} = -\frac{a_{\text{ho}}}{a_0} \quad \text{for } \ell = 0 \quad \text{and} \quad \rho\Psi(\rho, \mathcal{R})|_{\rho \rightarrow 0} = 0 \quad \text{for } \ell > 0 \quad (\text{S.7})$$

for the two-particle wave function $\Psi(\rho, \mathcal{R})$, where a_0 is the s -wave scattering length of the particle-particle interaction. Next, we determine and use the eigenfunctions of $\hat{H}_{\mathcal{R}}$ and \hat{H}_{ρ} as basis functions to finally compute the eigenenergies and eigenstates of the two-particle Hamiltonian $\hat{H} = \hat{H}_0 + s\hat{W}$.

CoM Basis Functions

The angular part of the CoM Hamiltonian $\hat{H}_{\mathcal{R}}$ can be separated by recalling that the eigenfunctions of the angular momentum operator \hat{L}^2 are the spherical harmonics $Y_{LM}(\Theta, \Phi)$ with the eigenvalues $L(L+1)$ and $L = 0, 1, 2, \dots$. Hence, the full eigenfunctions of $\hat{H}_{\mathcal{R}}$ are given by $\psi_{\text{CoM}}(\mathcal{R}, \Theta, \Phi) = (1/\mathcal{R})u_{n_{\mathcal{R}}L}(\mathcal{R})Y_{LM}(\Theta, \Phi)$, where the functions $u_{n_{\mathcal{R}}L}$ obey the radial Schrödinger equation

$$-\frac{1}{4} \frac{d^2 u_{n_{\mathcal{R}}L}}{d\mathcal{R}^2} + \left[\frac{L(L+1)}{4\mathcal{R}^2} + (\mathcal{R} - s_0)^2 \right] u_{n_{\mathcal{R}}L}(\mathcal{R}) = \mathcal{E}_{n_{\mathcal{R}}L} u_{n_{\mathcal{R}}L}(\mathcal{R}). \quad (\text{S.8})$$

In general, s_0 may be set equal to s , but for our numerical computations, it is advantageous, to use also different values, see below. The solutions of Eq. (S.8) can be given in terms of the biconfluent Heun functions [2, 3]. However, we do not make use of this fact

and instead directly solve the eigenvalue problem using the ApproxFun Julia package [4] leveraging a Chebyshev-polynomial-based spectral method.

In the case of $s_0 = 0$ we reproduce the case of the spherically symmetric three-dimensional harmonic oscillator with the eigenenergies

$$\mathcal{E}_{n_{\mathcal{R}}L} = \frac{3}{2} + 2n_{\mathcal{R}} + L \quad (\text{S.9})$$

and the corresponding wave function

$$u_{n_{\mathcal{R}}L}(\mathcal{R}) = A_{n_{\mathcal{R}}L} \mathcal{R}^{L+1} e^{-\mathcal{R}^2} L_{n_{\mathcal{R}}}^{(L+\frac{1}{2})} \left(2\mathcal{R}^2 \right) \quad (\text{S.10})$$

represented in terms of the Laguerre polynomials $L_n^{(\alpha)}(z)$, with $A_{n_{\mathcal{R}}L}$ being the normalization constant.

Relative Basis Functions

Analogously to the CoM case, the eigenfunctions of \hat{H}_ρ are given by $\varphi(\rho, \theta, \phi) = (1/\rho)v_{n_\rho\ell}(\rho)Y_{\ell m}(\theta, \phi)$, where the functions $v_{n_\rho\ell}(\rho)$ obey the radial Schrödinger equation

$$-\frac{d^2 v_{n_\rho\ell}(\rho)}{d\rho^2} + \left[\frac{1}{4}\rho^2 + \frac{\ell(\ell+1)}{\rho^2} \right] v_{n_\rho\ell}(\rho) = \mathcal{E}_{n_\rho\ell} v_{n_\rho\ell}(\rho) \quad (\text{S.11})$$

and are subject to the boundary conditions

$$\frac{1}{v_{n_\rho\ell}(\rho)} \frac{d}{d\rho} v_{n_\rho\ell}(\rho) \Big|_{\rho \rightarrow 0} = -\frac{a_{\text{ho}}}{a_0} \quad \text{for } \ell = 0 \quad (\text{S.12a})$$

and

$$v_{n_\rho\ell}(0) = 0 \quad \text{for } \ell > 0. \quad (\text{S.12b})$$

For $\ell > 0$ we again reproduce the spherically symmetric three-dimensional harmonic oscillator with the eigenenergies

$$\mathcal{E}_{n_\rho\ell}(\rho) = \left(\frac{3}{2} + 2n_\rho + \ell \right) \quad (\ell > 0) \quad (\text{S.13})$$

and the wave functions

$$v_{n_\rho\ell}(\rho) = A_{n_\rho\ell} \rho^{\ell+1} e^{-\frac{\rho^2}{4}} L_{n_\rho}^{(\ell+\frac{1}{2})} \left(\frac{\rho^2}{2} \right) \quad (\ell > 0), \quad (\text{S.14})$$

where $A_{n_\rho\ell}$ is the normalization constant.

In the case $\ell = 0$, the solutions are best written in terms of the parabolic cylinder functions $D_\nu(x)$

$$v_{n_\rho 0}(\rho) = A_{n_\rho 0}(a_0) D_{\mathcal{E}_{n_\rho 0}(a_0) - \frac{1}{2}}(\rho), \quad (\text{S.15})$$

where $A_{n_\rho 0}(a_0)$ is the normalization constant, whereas the energies $\mathcal{E}_{n_\rho 0}(a_0)$ are determined as the roots of the transcendental equation

$$\sqrt{2} \frac{\Gamma\left(\frac{3}{4} - \frac{1}{2}\mathcal{E}_{n_\rho 0}\right)}{\Gamma\left(\frac{1}{4} - \frac{1}{2}\mathcal{E}_{n_\rho 0}\right)} = -\frac{a_{\text{ho}}}{a_0}. \quad (\text{S.16})$$

This equation can be derived by inserting the asymptotic expansion of $v_{n_\rho 0}(\rho)$ as $\rho \rightarrow 0$, Eq. (S.15), into Eq. (S.12a), or by the method used in the original paper [5]. Due to numerical difficulties at the evaluation of the parabolic cylinder functions for negative orders $\nu < 0$, we resort to the numerical solution of the eigenvalue problem, Eqs. (S.11) and (S.12), with the help of the Julia ApproxFun package [4]. For $0 < a_0/a_{\text{ho}} < 1$ we obtain from Eq. (S.16) the asymptotic expansion for the ground state energy

$$\mathcal{E}_{00} = -\frac{1}{\alpha_0^2} + \frac{\alpha_0^2}{8} + \frac{7\alpha_0^6}{128} + \mathcal{O}(\alpha_0^{10}). \quad (\text{S.17})$$

Here made use of the asymptotic expansion of the Gamma function for large arguments and the iterative method to solve the equation.

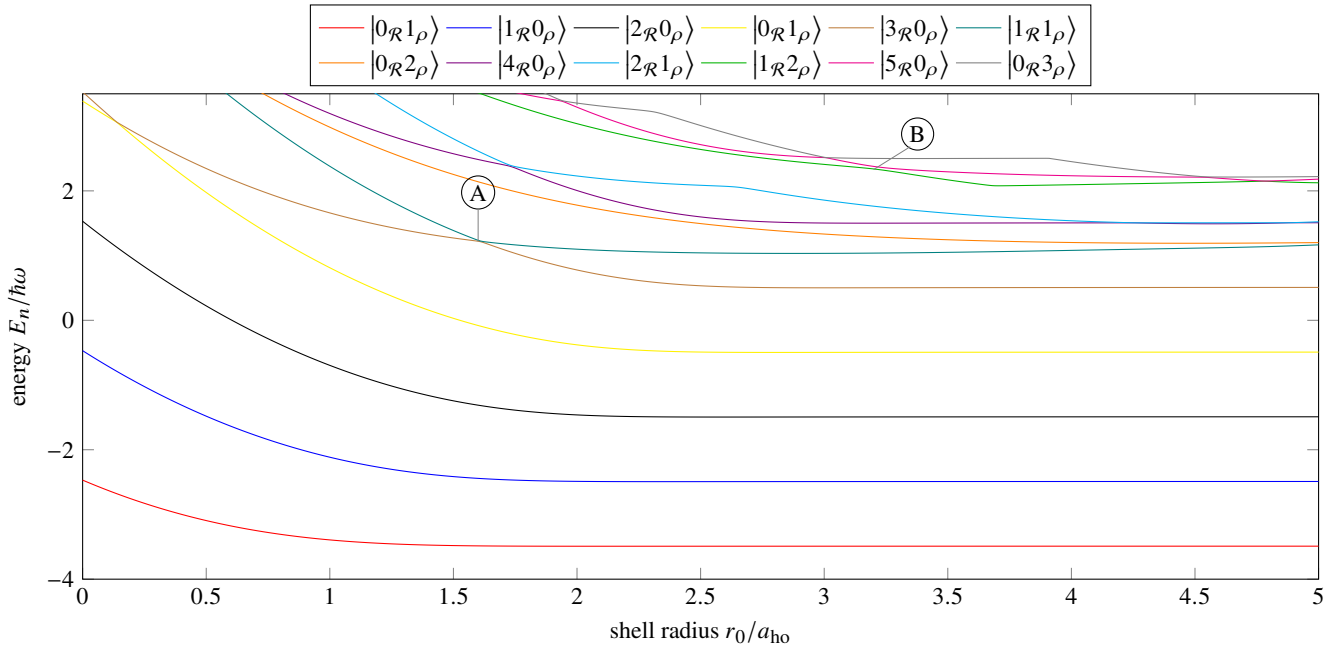


Figure S.1. Spectrum of the two-particle Hamiltonian Eq. (S.1) for zero total angular momentum, that is with $L = \ell = 0$, as a function of the shell radius r_0 obtained by the exact numerical diagonalization. For the labeling of the energies, we use the quantum numbers $n_{\mathcal{R}}$ and n_{ρ} of the corresponding states $|n_{\mathcal{R}}, n_{\rho}\rangle$ at $r_0 = 0$. The states with the lowest energies contain the ground state of the relative motion, corresponding to a molecule on the shell, and show the spectrum of an harmonic oscillator with constant distance between the energy levels for large shell radii $r_0 \gg a_{ho}$. Two symbols (A) and (B) identify the avoided crossings discussed in the Letter.

Diagonalizaion

Having obtained the functions $u_{n_{\mathcal{R}}L}(\mathcal{R})$ and $v_{n_{\rho}\ell}(\rho)$, we are in the position to expand the coupling operator \hat{W} , Eq. (S.6), in \hat{H} in terms of these functions. We make use of the fact that each summand of \hat{W} factors in a radial and angular part, cf. Eq. (S.2). The matrix elements of the latter can be given exactly in terms of the Clebsch-Gordon coefficients, while the matrix elements determined by the functions of \mathcal{R} and ρ are obtained by two-dimensional integration based on the Gauss-Lobatto scheme.

In order to save computational time during scanning over different values of s , we do not compute new basis functions and even more expensive matrix elements for each value of s . Instead, we just compute them for fixed values s_0 and rewrite the original Hamiltonian in the form

$$\hat{H} = \hat{H}_0 + s\hat{W} - 2\hat{\mathcal{R}}\delta s + 2s_0\delta s + (\delta s)^2 \quad (\text{S.18})$$

with $\delta s = s - s_0$. Now have to additionally calculate the matrix elements of the CoM position operator $\hat{\mathcal{R}}$. In the chosen basis only \hat{W} and $\hat{\mathcal{R}}$ contain off-diagonal terms. We use the ARPACK library to calculate the eigenenergies and eigenfunctions of Eq. (S.18) in a matrix free fashion, by exploiting the sum-of-products structure of \hat{W} and the tensor product structure of $\hat{\mathcal{R}}$.

In Fig. S.1, we show the spectrum of Eq. (S.1) for states with zero total angular momentum obtained by the diagonalization procedure described above. The states originating from the ground state of the relative motion, i. e. the bound state, show the spectrum of an one-dimensional harmonic oscillator with a constant level spacing of $\hbar\omega$, for sufficiently large r_0 . However, for $r_0 = 0$ the energy spacing is $2\hbar\omega$, which corresponds to the spherical three-dimensional harmonic oscillator.

APPROXIMATE SOLUTION

In order to obtain the approximate solutions for the eigenenergies and eigenfunctions, we use hyperspherical coordinates, namely the hyperradius $\xi = \sqrt{\frac{1}{2}r^2 + 2R^2}$, the hyperangle $\chi = \arctan(r/2R)$, the spherical angles θ and ϕ of \mathbf{r} , as well as Θ and Φ of \mathbf{R} . In these coordinates [6], the two-particle Hamiltonian reads

$$\hat{H} = -\frac{\hbar^2}{2m} \left(\frac{\partial^2}{\partial \xi^2} + \frac{5}{\xi} \frac{\partial}{\partial \xi} - \frac{\hat{\Lambda}^2}{\xi^2} \right) + \frac{m\omega^2}{2} (\xi - \xi_0)^2 + \mathcal{V}_c \quad (\text{S.19})$$

with $\xi_0 = \sqrt{2}r_0$. Here, $\hat{\Lambda}^2 = -\hat{\Lambda}_0^2 + \mathcal{W}_\xi(\chi)$ consists of the Laplacian operator on the six-dimensional hypersphere

$$\hat{\Lambda}_0^2 = \frac{\partial^2}{\partial \chi^2} + 4 \cot(2\chi) \frac{\partial}{\partial \chi} - \frac{\hat{\ell}^2}{\sin^2(\chi)} - \frac{\hat{L}^2}{\cos^2(\chi)} \quad (\text{S.20})$$

and the potential

$$\mathcal{W}_\xi(\chi) = \frac{2\xi^3\xi_0}{a_{\text{ho}}^4} \left[1 - \frac{2 + \sin^2(2|\frac{\pi}{4} - \chi|)}{3 \cos(\frac{\pi}{4} - |\frac{\pi}{4} - \chi|)} \right] \quad (\text{S.21})$$

depending on ξ and χ . The third term [1]

$$\mathcal{V}_c = -m\omega^2\xi\xi_0 \sum_{l=1}^{\infty} \frac{\sin^{2l}(\frac{\pi}{4} - |\chi - \frac{\pi}{4}|)}{\cos^{2l+1}(\frac{\pi}{4} - |\chi - \frac{\pi}{4}|)} \left[\frac{\sin^2(\frac{\pi}{4} - |\chi - \frac{\pi}{4}|)}{4l+3} - \frac{\cos^2(\frac{\pi}{4} - |\chi - \frac{\pi}{4}|)}{4l-1} \right] \frac{4\pi}{4l+1} \sum_{\mu=-2l}^{2l} Y_{2l,\mu}(\theta, \phi) Y_{2l,\mu}^*(\Theta, \Phi) \quad (\text{S.22})$$

in Eq. (S.19) connects all degrees of freedom.

By neglecting the coupling term \mathcal{V}_c and using the spherical harmonics $Y_{LM}(\Theta, \Phi)$ and $Y_{\ell m}(\theta, \phi)$, we can separate the spherical angles θ, ϕ, Θ , and Φ from the ξ and χ variables and arrive at

$$\Psi_{n_\xi n_\chi LM \ell m}(\xi, \chi, \Theta, \Phi, \theta, \phi) = \frac{U_{n_\xi n_\chi L \ell}(\xi) V_{n_\chi L \ell, \xi}(\chi)}{\xi^{5/2} \sin(2\chi)} Y_{LM}(\Theta, \Phi) Y_{\ell m}(\theta, \phi) \quad (\text{S.23})$$

for the two-particle eigenfunction. Here the functions $V_{n_\chi L \ell, \xi}(\chi)$ obey the hyperangular Schrödinger equation

$$-\frac{\partial^2}{\partial \chi^2} V_{n_\chi L \ell, \xi}(\chi) + \left[\mathcal{W}_\xi(\chi) + \frac{L(L+1)}{\cos^2(\chi)} + \frac{\ell(\ell+1)}{\sin^2(\chi)} - 4 \right] V_{n_\chi L \ell, \xi}(\chi) = \lambda V_{n_\chi L \ell, \xi}(\chi) \quad (\text{S.24})$$

with the Bethe-Peierls boundary condition

$$\frac{1}{V_{n_\chi L \ell, \xi}(\chi)} \frac{d}{d\chi} V_{n_\chi L \ell, \xi}(\chi) \Big|_{\chi \rightarrow 0} = -\frac{\sqrt{2}\xi}{a_0} \quad \text{for } \ell = 0. \quad (\text{S.25a})$$

and

$$V_{n_\chi L \ell, \xi}(0) = 0 \quad \text{for } \ell > 0. \quad (\text{S.25b})$$

The hyperangular quantum number n_χ corresponds to the number of nodes in the hyperangular direction. In general, Eq. (S.24) with the conditions Eq. (S.25) can only be solved numerically. As with the basis functions for the exact diagonalization, we have used the Julia ApproxFun package [4] to obtain the eigenfunctions $V_{n_\chi L \ell, \xi}(\chi)$ with the corresponding eigenvalues $\lambda = \lambda(n_\chi, L, \ell, \xi)$.

Finally, we assume that the hyperangular wave function $V_{n_\chi L \ell, \xi}(\chi)$ changes only adiabatically with the hyperradius ξ , such that terms involving $\frac{\partial}{\partial \xi} V_{n_\chi L \ell, \xi}(\chi)$ can be neglected. This procedure is similar to the Born-Oppenheimer approximation [7] and allows us to calculate the two-particle energy $E_{n_\xi n_\chi L \ell}$ from the corresponding hyperradial Schrödinger equation

$$-\frac{\hbar^2}{2m} \frac{\partial^2 U_{n_\xi n_\chi L \ell}(\xi)}{\partial \xi^2} + \left[\frac{\hbar^2}{2m} \frac{\lambda(n_\chi, L, \ell, \xi) + 15/4}{\xi^2} + \frac{m\omega^2}{2} (\xi - \xi_0)^2 \right] U_{n_\xi n_\chi L \ell}(\xi) = E_{n_\xi n_\chi L \ell} U_{n_\xi n_\chi L \ell}(\xi) \quad (\text{S.26})$$

for the function $U_{n_\xi n_\chi L \ell}(\xi)$.

To solve Eq. (S.26) numerically, we have used a sin-based Lagrange mesh [8, 3.7.2.] and then employed the ARPACK package. The mesh method allows us to restrict the number of required evaluations of $\lambda(n_\chi, \xi, L, \ell)$, in contrast to the previously applied spectral method.

In the limit of large shell radii, as well as for $L = \ell = 0$, we are able to derive approximate analytical expressions for the energies and the wave functions involving the hyperangular ground state. To do it, we expand the potential $\mathcal{W}_\xi(\chi)$, Eq. (S.21), around $\chi = 0$ and find

$$\mathcal{W}_\xi(\chi) = \frac{\xi^3 \xi_0}{3a_{\text{ho}}} \chi^2 + \mathcal{O}(\chi^3). \quad (\text{S.27})$$

Then Eq. (S.24) takes the form

$$\frac{\partial^2}{\partial \chi^2} V_0(\chi) + \left[-\frac{\xi^3 \xi_0}{3a_{\text{ho}}^4} \chi^2 + 4 + \lambda \right] V_0(\chi) = 0 \quad (\text{S.28})$$

with the solutions

$$D_\nu \left[\pm \left(\frac{2}{3} \xi^3 \xi_0 \right)^{\frac{1}{4}} \chi \right] \quad (\text{S.29})$$

in terms of the parabolic cylinder functions, where the order ν is related to the eigenvalue λ

$$\lambda = -4 + \frac{(2\nu + 1)\sqrt{\xi^3 \xi_0}}{\sqrt{3}a_{\text{ho}}^2}. \quad (\text{S.30})$$

The values of ν are then the roots of the transcendental equation

$$-\frac{\sqrt{2}\Gamma\left(\frac{1}{4}(3 - \sqrt{3}\nu)\right)}{\sqrt[4]{3}\Gamma\left(\frac{1}{4}(1 - \sqrt{3}\nu)\right)} = \frac{a_{\text{ho}}}{a_0}, \quad (\text{S.31})$$

resulting from the Bethe-Peierls boundary condition Eq. (S.25a).

For $0 < \frac{a_0}{a_{\text{ho}}} < 1$ we find for the ground state

$$\lambda = \xi^2 \left[-\frac{2}{a_0^2} - 4 + \frac{a_0^2}{12a_{\text{ho}}^4} + \mathcal{O}(a_0^6) \right]. \quad (\text{S.32})$$

When we insert this expression into Eq. (S.26), we obtain

$$-\frac{\hbar^2}{2m} \frac{\partial^2 U_{n_\xi 0}(\xi)}{\partial \xi^2} + \left[-\frac{\hbar^2}{2m} \frac{1}{4\xi^2} + \frac{m\omega^2}{2} (\xi - \xi_0)^2 + \frac{\hbar^2}{m} \left(-\frac{1}{a_0^2} + \frac{a_0^2}{24a_{\text{ho}}^4} \right) \right] U_{n_\xi 0}(\xi) = E_{n_\xi 0} U_{n_\xi 0}(\xi). \quad (\text{S.33})$$

For large ξ_0 the ξ^{-2} term may be neglected, such that only the shifted harmonic potential remains. Hence we find the approximated hyperradial spectrum

$$E_{n_\xi 0} \approx \hbar\omega \left(n_\xi + \frac{1}{2} \right) + \frac{\hbar^2}{m} \left(-\frac{1}{a_0^2} + \frac{a_0^2}{24a_{\text{ho}}^4} \right) + \mathcal{O}\left(\frac{1}{\xi_0^2}\right). \quad (\text{S.34})$$

This corresponds to the spectrum of a one-dimensional oscillator that is shifted by the binding energy.

* moritz.carmesin@uni-ulm.de

- [1] D. A. Varshalovich, A. N. Moskalev, and V. K. Khersonskii, *Quantum Theory of Angular Momentum* (WORLD SCIENTIFIC, 1988).
- [2] A. Ronveaux and F. M. Arscott, *Heun's differential equations* (Oxford University Press, 1995).
- [3] J. Karwowski and H. A. Witek, Biconfluent heun equation in quantum chemistry: Harmonium and related systems, *Theoretical Chemistry Accounts* **133**, 1494 (2014).
- [4] S. Olver and A. Townsend, A practical framework for infinite-dimensional linear algebra, in *Proceedings of the 1st Workshop for High Performance Technical Computing in Dynamic Languages – HPTCDL '14* (IEEE, 2014).
- [5] T. Busch, B.-G. Englert, K. Rzazewski, and M. Wilkens, Two Cold Atoms in a Harmonic Trap, *Foundations of Physics* **28**, 549 (1998).
- [6] T. K. Das, *Hyperspherical Harmonics Expansion Techniques: Application to Problems in Physics*, 1st ed., Theoretical and Mathematical Physics (Springer-Verlag, 2015).
- [7] M. Born and R. Oppenheimer, Zur Quantentheorie der Molekeln, *Annalen der Physik* **389**, 457 (1927).
- [8] D. Baye, The Lagrange-Mesh Method, *Physics Reports* **565**, 1 (2015).